Droplet Velocity Fluctuations in Thermally Stimulated Continuous Liquid Jets

Jeremy Grace and Giuseppe Farruggia); Eastman Kodak Company; Rochester, New York

Abstract

The interesting phenomenon of the breakup of continuous liquid jets into droplets has significant practical applications, including inkjet printing. Regardless of print mode (i.e., on-demand vs. continuous), as applications require increasingly precise droplet control, inherent noise in the breakup process is becoming an area of increasing interest. We examine jitter to infer the underlying velocity fluctuations in thermally stimulated continuous fluid jets. Based upon comparisons of jets having different diameters D, as well as jets stimulated at different frequencies (hence different wavelengths λ), we find that the jitter depends significantly upon the dimensionless wavelength λ/D, showing a minimum at the natural frequency of the jet (corresponding to λ/D = 5) and a marked enhancement over the range 6 < λ/D < 8. We present an analysis of the frequency dependence of the jitter in the context of a simple model for growth of radial perturbations on the jet.

Introduction

The breakup of liquid jets has fascinated scientists for centuries and has found applications in a broad variety of disciplines and technologies [1]. Jet breakup, or droplet formation, is a consequence of the Rayleigh-Plateau instability, which is driven by capillary forces acting to reduce the surface area of the jet [2]. Background fluctuations can feed this instability to produce spontaneous jet breakup. Intentionally imposed disturbances, such as mechanical or thermal pulses, drive this instability to produce particular droplet patterns. While imposed disturbances dominate the jet breakup process, underlying fluctuations can affect the velocity of a newly formed droplet.

In this work, we study fluctuations in droplet velocity in streams of an aqueous solution jetted from microfabricated nozzle arrays. The jets are thermally stimulated by applying square wave voltage waveforms to resistive heaters that surround the nozzle bores. Breakup lengths and the positional variation of successive droplets are directly measured using stroboscopic photography. From these respective observables, implied radial perturbations and velocity fluctuations are determined. The velocity fluctuations and breakup behavior are studied as a function of the droplet wavelength λ, by varying the repetition frequency of the voltage waveform or the fluid velocity (which is controlled by the inlet pressure).

Experimental Details

Jetting modules were mounted on fixtures equipped with fluidic supply tanks and connections, motorized translation stages, and a large focal length (approximately 35 mm) microscope (see Fig. 1). Driving voltage waveforms were applied to the heaters by control of CMOS logic located directly on the nozzle array chips. Using a pulse delay generator (Stanford Research Model DG535) a light emitting diode (LED) strobe light was synchronized with the driving voltage waveform to enable stroboscopic observation of droplets. A combination of intense LED (with an enhanced driver, based upon field effect transistors) and a sensitive CCD camera (Watec 902H2 "supreme") enabled "single-shot" images, wherein single LED flashes were sufficiently short and sufficiently intense to produce a still image of the jet and/or droplets in flight.

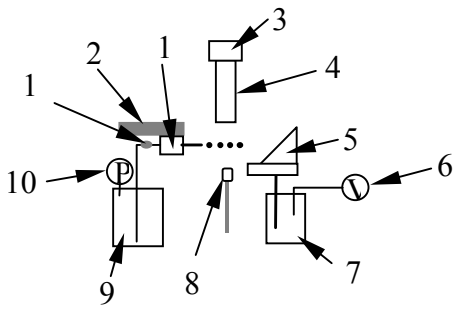

Figure 1. Schematic of setup used to capture images of droplets. 1) jetting module; 2) translation stage(s); 3) CCD camera; 4) microscope; 5) droplet catcher; 6) vacuum source; 7) fluid waste tank; 8) LED strobe light; 9) fluid supply tank(s); 10) pressure source; 11) in-line filter.

The average droplet velocity as a function of distance from breakup was measured by using multiple (roughly 100) flashes per frame and dividing the spacing for each droplet pair by the driving period. The average droplet velocity at breakup was then found by extrapolation to the breakoff point. The jet velocity was calculated from the droplet velocity at breakup and the surface tension (see below) and used to compute the volumetric flow. The jet radius was estimated by comparing measured and computed volumetric flows at several inlet pressures, bringing them into agreement at each pressure by fitting the jet radius to a linear function of pressure and minimizing the mean-squared error between measured and calculated flow values.

The fluid used in this work is water with added surfactant (Surfynol 465, 0.05% by wt), biostatic agent (Proxel GXL, 0.1% by wt.), and acetic acid (0.001% by wt.).

Jetting Module

Silicon chips were prepared with arrays of 32 nozzles (having a pitch of 600 npi) surrounded by polysilicon heaters, using standard lithographic techniques. A schematic of the nozzle bore

geometry is shown in Fig. 2. Oval channels are formed using a deep reactive ion etch process. Membrane material (silicon dioxide, ~5 μm thick), polysilicon heaters, and gold leads are deposited and patterned by standard thin-film deposition and etching processes.

Bore diameters for the devices studied are nominally 6.9 and 8.6 μm. For the 6.9 μm diameter nozzles, respective inner and outer heater diameters are roughly 8.7 and 13.1 μm. For the 8.6 μm nozzles, the respective inner and outer heater diameters are roughly 10.4 and 15.8 μm.

The nozzle array chips were affixed to a fluid delivery manifold and connected to a flexible cable, which was then attached to the drive electronics.

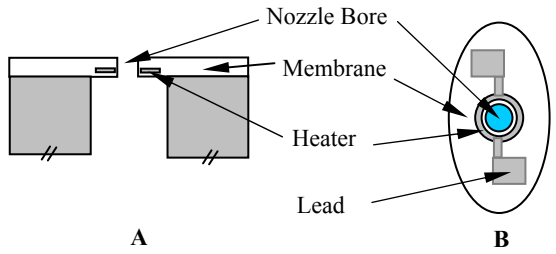

Figure 2. Schematic of nozzle geometry in nozzle array. A) Side cross-sectional view. B) Plan view. Fluidic channels having an oval cross section are etched in a silicon wafer. The nozzle bores are centered over the channels and etched through a silicon oxynitride membrane, which contains embedded polysilicon heaters.

CMOS circuitry located on the chips containing the nozzle arrays is used to address the resistive heaters and supply the same drive voltage to each heater. A system clock is used to control pulse widths for the heat pulse waveform. In this work, a 30% duty cycle positive voltage pulse was used to drive the heaters, except for the lowest two frequencies, where the duty cycle was reduced to 26%, and the voltage increased to maintain the same average dissipated power (roughly 9 mW). For the measurements presented here, only one heater near the center of the array was excited.

Jitter Measurements

Images of several droplets are taken in single-shot mode. (The number of droplets per frame ranges from 5 at the lowest frequencies to 20 at the highest frequencies.) Image data are captured using a NIMAQ 1410 image capture card from National Instruments. The image capture and analysis is controlled using a graphical user interface written in LabView™. Each image is processed to find the locations of the drop centers. Values for the individual drop positions, the average drop positions, and the spacing between neighboring drops are stored in an array. The array is updated and expanded as each successive image is acquired every 1/30 s. After data for 1000 successive images has been stored, the average values and standard deviations are output to a file. Process conditions (i.e., power, frequency, or inlet pressure) are then changed, and the measurements are repeated.

The camera position is set close enough to jet breakup that the observed jitter increases linearly with position. Slopes of position jitter vs. distance from breakup provide the basis for determination of the velocity jitter.

The droplets released from the jet at breakoff have a distribution of velocities v. As the droplets travel further from breakoff, the variation in position at a given time from breakoff increases in proportion to the distance from breakoff:

$$\frac{\sigma_v}{v} = \frac{\sigma_x}{x}, \tag{1}$$

where σ_v and σ_x are respective velocity and position standard deviations.

When examining positional variation in droplets in a stream it is important to consider that, in addition to the uncorrelated jitter in the droplet velocity, the variation may have contributions that affect many droplets similarly. For example, low-frequency vibrations may cause all drops in the field of view to move together relative to the camera frame. As the uncorrelated droplet jitter is related to the fundamental behavior of the jet, and the correlated jitter can be caused by external and potentially highly variable factors, it is helpful to measure the uncorrelated jitter clear of the correlated droplet jitter.

From Eq. 1 it can be shown that

$$\sigma_x = \langle d \rangle \frac{\sigma_v}{v} = \frac{\sigma_\Delta}{\sqrt{\left(2 + \frac{4\lambda}{\langle d \rangle} + \frac{2.5\lambda^2}{\langle d \rangle^2}\right)}}, \tag{2}$$

where σ_x is the standard deviation in droplet position at the mean distance $<d>$ from breakup for a pair of neighboring drops, σ_Δ is the standard deviation in spacing between neighboring drops, and λ is the drop formation wavelength. This result is found by expressing the neighboring droplet positions as products of their velocities and times from breakup, expressing the standard deviation in breakup time in terms of the standard deviation in velocity, and noting that the ratio of jet velocity v_{jet} to λ_{jet} (the drop formation wavelength along the jet) is the drop generation frequency, which is invariant before and after breakup.

The relationship between variation in breakup time and variation in velocity comes from the relation between variation in breakup length ($\delta l = v\sigma_t$) relative to the drop formation wavelength and the variation in velocity relative to the average velocity:

$$\frac{v_{jet}\sigma_t}{\lambda_{jet}} = \frac{\sigma_v}{v}. \tag{3}$$

Effective Radial Perturbation

The calculation of effective radial perturbations from breakup lengths is based upon a simplification of an analytical treatment of liquid microjets by Furlani [3] proposed by A. Clarke [4]. In this

approach, the amplitude ξ of a periodic radial disturbance on a jet grows exponentially according to

$$\xi = \xi_i \exp(\alpha t), \quad (4)$$

where ξ_i is the initial perturbation, α is the growth rate, and *t* is the time. The decaying term (negative growth rate) is neglected in this approach.

The growth rate depends upon fluid properties, jet radius *R*, and stimulation frequency:

$$\alpha^2 + \frac{3\mu(kR)^2}{\rho R^2}\alpha - \frac{\sigma}{2\rho R^3}\left(1-(kR)^2\right)(kR)^2 = 0 \quad (5)$$

Here, μ is the dynamic viscosity, ρ is the fluid density, σ is the surface tension, and $kR\ (= \pi D/\lambda)$ is the dimensionless wave number. The growth rate exhibits a maximum at the Rayleigh frequency (corresponding to a value of λ/D of approximately 5 for the fluid studied here). In order to specify the wave number, the jet velocity and stimulation frequency must be known.

The jet velocity v_{jet} can be related to the drop velocity at breakup v_0 by [5]:

$$v_0 = v_{jet} - \frac{\sigma}{\rho v_{jet} R}, \quad (6)$$

Finally, the initial perturbation or the breakup time t_B can be determined from the breakup length L_B, the growth rate, and the jet velocity according to:

$$L_B = \frac{v_{jet}}{\alpha}\ln\left(\frac{R}{\xi_i}\right) = t_B v_{jet} \quad (7)$$

This expression is found by solving Eq. 6 for t_B with $\xi = R$ at the breakup time t_B.

As the excitation voltage provided to the heaters is a square wave with 30% duty cycle, we must consider the additional Fourier components in the applied disturbance. Only the first few of these components are needed, as the jet naturally rejects frequencies higher than a cut-off frequency at which no real growth rate α can be calculated. Roughly speaking, for dimensionless wavelength values $\lambda/D < 6$, no additional components are needed. For $6 < \lambda/D < 10$, a component at twice the fundament frequency is needed. Between $\lambda/D = 10$ and $\lambda/D = 15$, components at thrice and four times the fundamental frequency are added.

Disturbances of the form

$$\xi = \xi_i \exp(\alpha_i t)\cos(\omega_i t + \varphi_i) \quad (8)$$

are summed to produce an effective perturbation ξ_{eff} that grows at an effective rate α_{eff} as in Eq. 4. Here, the individual components have values of initial perturbation, growth rate, angular frequency ω, and relative phase ϕ, indexed by *i*. The relative values of ξ_I and the relative phases ϕ_i are taken from the Fourier transform of the input waveform. The effective initial perturbation ξ_{eff} is proportional to the sum of the Fourier components ξ_i. The radial profile of the jet is obtained by subtracting the summed radial disturbances from the undisturbed jet radius *R*. Similarly, the effective profile is obtained by subtracting the right side of Eq. 4 from *R*, setting ξ_i equal to ξ_{eff} and using Eq. 7 to express α_{eff} in terms of ξ_i and the measured breakup length. ξ_{eff} is then scaled to produce the result that the envelope of the radial profile obtained from the summed components of Eq. 8 falls to zero at the breakup time. The value of α_{eff} (determined from ξ_{eff}) forces the envelope function of the radial profile obtained from Eq. 6 to fall to zero at the breakup time.

The expected velocity jitter (≡ δV/V) for a single-frequency excitation can be derived by using Eq. 7 to find the fluctuation in breakup time from a fluctuation $\delta\xi_i$ in initial perturbation, and then using conservation of momentum at breakup to relate the relative fluctuation in droplet mass to the relative velocity fluctuation. Thus, the velocity jitter is found to be:

$$\frac{\delta V}{V} = \frac{v_{jet}}{\lambda\alpha}\left(\frac{\delta\xi_i}{\xi_i}\right) \quad (9)$$

The experimentally measured jitter for the 30% duty square wave excitation will have additional effects arising from the relative growth of the background radial fluctuations and the applied radial perturbation. If the noise at the Rayleigh frequency is dominant, the expected jitter will be:

$$\frac{\delta V}{V} = \frac{v_{jet}}{\lambda\alpha_{eff}}\left(\frac{\delta\xi_0}{\xi_{eff}}\right)\frac{e^{\alpha_0 t_B}}{e^{\alpha_{eff} t_B}} = s\frac{\delta\xi_0}{R}\frac{e^{\alpha_0 t_B}}{e^{\alpha_{eff} t_B}}, \quad (10)$$

where the subscript *0* denotes the value at the Rayleigh frequency, *eff* denotes the effective value as described above, and *s* $(=Rv_{jet}/[\xi_{eff}\lambda\alpha_{eff}])$ is defined as a dimensionless stimulation parameter. If one considers a noise spectrum and integrates the growth factors over the noise spectrum, the noise contribution at the Rayleigh frequency is replaced by a term whose effective dependence upon the breakup time is similar and gives qualitatively similar results.

Results

Breakup length and velocity jitter are shown respectively in Figs. 3and 4 for stimulation at an average power of roughly 9 mW and driving frequencies corresponding to dimensionless wavelength values from 5 to 15. Comparison of the two figures suggests a correspondence between peaks in the breakup length and peaks in the jitter. Furthermore, data obtained at a fixed frequency of 353.5 kHz and at various jet velocities (varied by changing the inlet pressure) exhibit a similar, but less sharp peak in jitter at λ/D = 6.5. Additional data for a nominal nozzle diameter of 8.6 μm (estimated jet radius of 8.7 μm) exhibits the same primary peak in jitter at λ/D = 6.5.

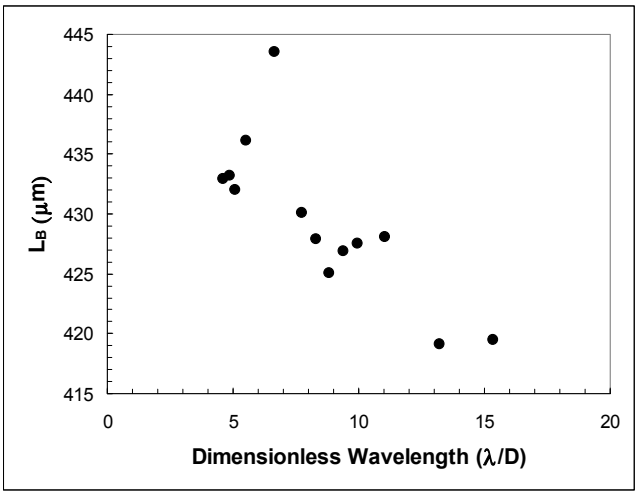

Figure 3. Breakup length as a function of dimensionless wavelength for thermally stimulated fluid jetted from a nominal 6.9 μm diameter nozzle.

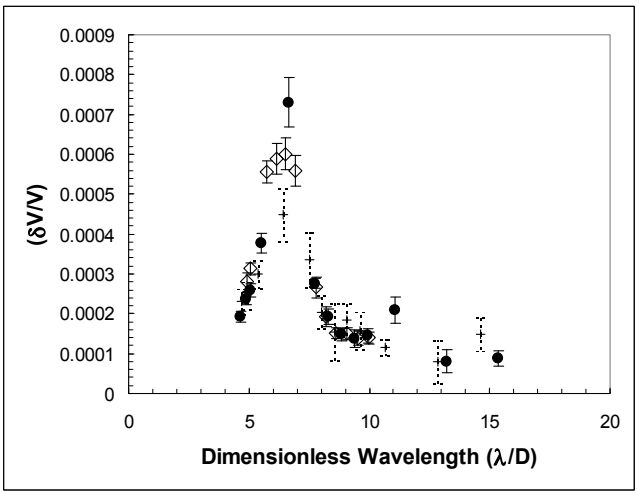

Figure 4. Velocity jitter as a function of dimensionless wavelength for thermally stimulated fluid jetted from a nominal 6.9 μm diameter nozzle: (•) frequency scan; (◊) velocity scan; and (+) frequency scan for fluid jetted from a nominal 8.6 μm diameter nozzle.

It is interesting to examine the jitter normalized to the stimulation parameter in Eq. 10, as one expects the jitter to scale with the inverse perturbation $1/\xi_{eff}$. Normalized jitter data are shown in Figs. 5 and 6 for the frequency scan and the velocity scan using the nominal 6.9 μm diameter nozzle. From Fig. 5 it appears that the normalized jitter exhibits a peak near λ/D = 7.5. This drop formation wavelength corresponds to creation of drops having 1.5 times the volume of the fundamental drops produced at the Rayleigh frequency. Stroboscopic images of the jet near breakup show that a satellite of substantial size is formed under these conditions. The normalized jitter falls to a local minimum near λ/D = 10, corresponding to production of two nearly equal drops per stimulation cycle. As the dimensionless wavelength is reduced towards the Rayleigh frequency, the size of the satellite decreases substantially.

Also shown in Figs. 5 and 6 are data for a range of input powers at fixed dimensionless wavelength values of 5 and 7.5. In these power scans, both the parameter *s* and the entire right side of Eq. 10 divided by $\delta\xi_0$ vary linearly with the inverse energy per drop (as calculated from the input power). By contrast, the jitter exhibits nonlinear behavior when plotted against inverse drop energy, *s*, or Eq. 10, more notably for the power scan at λ/D = 7.5. The normalized jitter plots suggest that the nonlinearities arise from the extreme dependence of normalized jitter on dimensionless wavelength. As power is increased in the power scans, the fluid velocity also increases, thereby increasing the dimensionless wavelength. While the jitter decreases with increasing power, the normalized jitter follows the trends seen in the frequency scans – near λ/D = 5 it increases with increasing wavelength, whereas above λ/D = 7.5 it decreases. These trends are consistent with the respective negative and positive quadratic effects observed in plots of jitter vs. inverse stimulation (inverse drop energy, *s*, or Eq. 10 divided by $\delta\xi_0$.) for λ/D values of 5 and 7.5.

Equation 10 can be fit to the data by adjusting the value of the radial fluctuation $\delta\xi_0$. The result of such a fit is shown in Figs. 5 and 6. While the fit to Eq. 10 reproduces most of the features seen in the experimental data, the details of the primary peak in jitter are not exactly reproduced. If the fit is brought into agreement in the low-wavelength range, it will fall below the observed jitter in the peak and beyond. It is possible that lowering the value of $\delta\xi_0$ to obtain agreement near λ/D = 5 is more appropriate, as the simple approach of Eq. 10 may be valid in this regime. At higher wavelengths, there may be additional noise contributions near the breakup point rather than near the nozzle bore and heater. These effects may be associated with filament formation and satellite formation phenomena during jet breakup, and they would not be accounted for by the perturbation growth model implicit in Eq. 10.

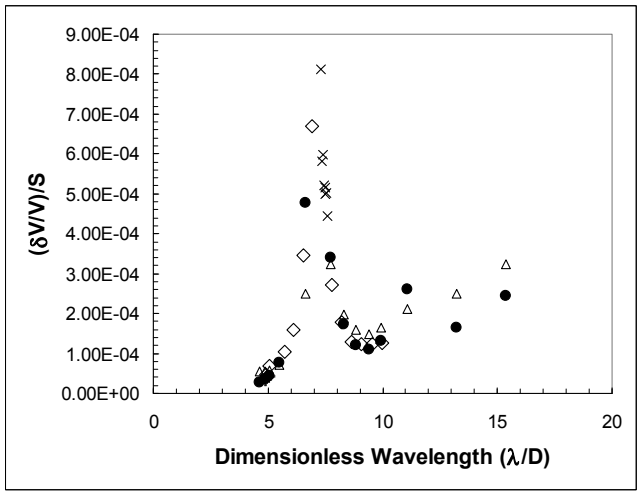

Figure 5. Normalized velocity jitter as a function of dimensionless wavelength for thermally stimulated fluid jetted from a nominal 6.9 μm diameter nozzle: (•) frequency scan; (◊) velocity scan; (+) power scan at λ/D = 5; (x) power scan at λ/D = 7.5; and (Δ) fit to Eq. 10.

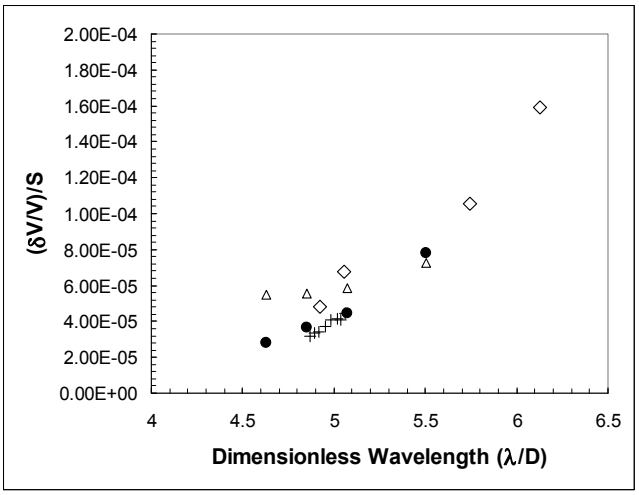

Figure 6. Normalized velocity jitter as a function of dimensionless wavelength for thermally stimulated fluid jetted from a nominal 6.9 µm diameter nozzle (expanded scale of Fig. 4): (•) frequency scan; (◊) velocity scan; (+) power scan at λ/D = 5; and (Δ) fit to Eq. 10.

Conclusions

Breakup length and jitter measurements on thermally stimulated aqueous microjets were obtained at various values of dimensionless wavelength λ/D. The wavelength was varied by changing the driving frequency and by changing the fluid velocity. In addition, measurements were performed at fixed λ/D values of 5 and 7.5 at various heater powers. Both the velocity jitter and the breakup length exhibit peaks in the response as a function of wavelength. The primary peak near $\lambda/D = 6.5$ is seen for different bore diameters and by scanning either the frequency or the velocity.

The normalized jitter (i.e., jitter divided by a stimulation parameter s, defined in the context of a simple radial perturbation model) suggests a peak in the ratio of background fluctuation to imposed perturbation near $\lambda/D = 7.5$, which corresponds to drop volumes of roughly 1.5 times the fundamental drops produced at the Rayleigh frequency. Beyond this peak, the normalized jitter appears to exhibit a local minimum near $\lambda/D = 10$, which corresponds to formation of two nearly equal droplets per stimulation cycle.

While the qualitative features of the jitter dependence upon drop formation wavelength are captured by the simple radial perturbation model, quantitative discrepancies may arise from additional noise occurring in the breakup process, possibly related to filament and satellite formation, which appear to be more severe at dimensionless wavelength values near 7.5.

Acknowledgments

The authors gratefully acknowledge Andrew Clarke for his guidance and many helpful discussions. The authors are also grateful to Justin Gao, Hrishikesh Panchawagh, and Kathleen Vaeth for many helpful discussions. Thanks also go to Darryl Tinney for writing the graphical user interface and other software support for the jitter and drop velocity measurements.

References

[1] J. Eggers and E. Villermaux, "Physics of Liquid Jets," Rep. Prog. Phys., 71, 1–79 (2008).

[2] T. E. Faber, Fluid Dynamics for Physicists (CUP, Cambridge, UK, 1995) pg. 295.

[3] E. P. Furlani, "Temporal Instability of Viscous Liquid Microjets with Spatially Varying Surface Tension," J. Phys. A: Math. Gen., 38, 263–276 (2005).

[4] Andrew Clarke, Eastman Kodak Company, private communication (2008).

[5] V. V. Krotov and A. I. Rusanov, Physicochemical Hydrodynamics of Capillary Systems (ICP, London, UK, 1999) pg. 271.

Author Biography

Jeremy M. Grace received his B.S. in Physics from MIT and his M.S. and Ph.D. in physics from the University of Illinois at Urbana-Champaign. After post-doctoral appointments at IBM and the Argonne National Laboratory, he joined the Research Laboratories at Eastman Kodak Company in Rochester, New York. At Kodak, he has worked in the areas of droplet generation in continuous fluid jets, plasma processing of materials, thin-film deposition processes, and plasma modification of polymer surfaces.

Giuseppe Farruggia attended the Rochester Institute of Technology in Rochester, New York. He joined the Research Laboratories at Eastman Kodak Company in Rochester, New York, as a Senior Research Technician. He has worked in the areas of droplet generation in continuous fluid jets, fabrication, characterization, and testing of organic light-emitting diode (OLED) devices, deposition, and properties of thin-film materials for optical recording media, and dynamic performance testing of the media.